Titolo rivista/libro: Modern pathology

Titolo articolo/sezione: PATZ1-Rearranged Tumors of the Central Nervous System: Characterization of a Pediatric Series of Seven Cases

Autore/i: Sabrina Rossi

ISSN: 0893-3952

DOI:

Anno: 2023

Volume:

Fascicolo:

Editore:

Pag. iniziale:

Pag. finale:

Mod Pathol 37 (2024) 100387

MODERN PATHOLOGY

UNITED STATES AND CANADIAN ACADEMY OF PATHOLOGY
Creating a Better Pathologist

Journal homepage: https://modernpathology.org/

Research Article

PATZ1-Rearranged Tumors of the Central Nervous System: Characterization of a Pediatric Series of Seven Cases

Sabrina Rossi[a,*], Sabina Barresi[a], Giovanna Stefania Colafati[b,c], Silvia Genovese[d], Chantal Tancredi[a], Valentino Costabile[e], Sara Patrizi[f], Isabella Giovannoni[a], Sofia Asioli[g], Pietro Luigi Poliani[h], Marina Paola Gardiman[i], Antonello Cardoni[a], Giada Del Baldo[f], Manila Antonelli[j], Francesca Gianno[j,k], Eleonora Piccirilli[b,c], Giorgia Catino[d], Licia Martucci[d], Denise Quacquarini[a], Francesco Toni[l], Fraia Melchionda[m], Elisabetta Viscardi[n], Mino Zucchelli[o], Sandro Dal Pos[p], Enza Gatti[q], Roberto Liserre[q], Elisabetta Schiavello[r], Francesca Diomedi-Camassei[a], Andrea Carai[s], Angela Mastronuzzi[f], Marco Gessi[t], Caterina Giannini[g,u], Antonio Novelli[d], Andrea Onetti Muda[v], Evelina Miele[f,*], Viola Alesi[d], Rita Alaggio[a,w]

[a] *Pathology Unit, Department of Laboratories, Bambino Gesù Children's Hospital, IRCCS, Rome, Italy;* [b] *Imaging Department, Bambino Gesù Children's Hospital, IRCCS, Rome, Italy;* [c] *Department of Neuroscience, Imaging and Clinical Sciences (DNISC), University "Gabriele D'Annunzio" of Chieti-Pescara, Chieti, Italy;* [d] *Laboratory of Medical Genetics, Translational Cytogenomics Research Unit, Bambino Gesù Children's Hospital, IRCCS, Rome, Italy;* [e] *Multimodal Research Area, Unit of Microbiology and Diagnostics in Immunology, Bambino Gesù Children's Hospital, IRCCS, Rome, Italy;* [f] *Onco-Hematology, Cell Therapy, Gene Therapies and Hemopoietic Transplant, Bambino Gesù Children's Hospital, IRCCS, Rome, Italy;* [g] *Department of Biomedical and Neuromotor Sciences (DIBINEM)-Surgical Pathology Section-Alma Mater Studiorum – University of Bologna, Bologna, Italy;* [h] *Pathology Unit, San Raffaele Hospital Scientific Institute, Vita-Salute San Raffaele University, Milan, Italy;* [i] *Surgical Pathology and Cytopathology Unit, Department of Medicine, University Hospital of Padua, Padua, Italy;* [j] *Department of Radiology, Oncology and Anatomic Pathology, University La Sapienza, Rome, Italy;* [k] *IRCCS Neuromed, Pozzilli, Isernia, Italy;* [l] *Neuroradiology Unit, IRCCS Istituto delle Scienze Neurologiche di Bologna, Bologna, Italy;* [m] *SSD Oncoematologia Pediatrica, IRCCS AOU Policlinico S.Orsola, Bologna, Italy;* [n] *Department of Pediatrics, Azienda Ospedale-Università di Padova, Padova, Italy;* [o] *Paediatric Neurosurgery, IRCCS Istituto delle Scienze Neurologiche di Bologna, Bologna, Italy;* [p] *Department of Radiology, Azienda Ospedale-Università di Padova, Padova, Italy;* [q] *Department of Radiology, Neuroradiology Unit, ASST Spedali Civili University Hospital, Brescia, Italy;* [r] *Pediatric Oncology Unit, Fondazione IRCCS Istituto Nazionale dei Tumori, Milan, Italy;* [s] *Neurosurgery Unit, Bambino Gesù Children's Hospital, IRCCS, Rome, Italy;* [t] *Neuropathology Unit, Pathology Division, Fondazione Policlinico Universitario A. Gemelli IRCCS, Università Cattolica S.Cuore, Rome, Italy;* [u] *Department of Anatomic Pathology, Mayo Clinic, Rochester, Minnesota;* [v] *Bambino Gesù Children's Hospital, IRCCS, Rome, Italy;* [w] *Department of Medico-surgical Sciences and Biotechnologies, Sapienza University, Rome, Italy*

ARTICLE INFO

Article history:
Received 14 August 2023
Revised 28 October 2023
Accepted 6 November 2023
Available online 23 November 2023

Keywords:
brain sarcomas
chromothripsis

ABSTRACT

PATZ1-rearranged sarcomas are well-recognized tumors as part of the family of round cell sarcoma with *EWSR1*-non-ETS fusions. Whether *PATZ1*-rearranged central nervous system (CNS) tumors are a distinct tumor type is debatable. We thoroughly characterized a pediatric series of *PATZ1*-rearranged CNS tumors by chromosome microarray analysis (CMA), DNA methylation analysis, gene expression profiling and, when frozen tissue is available, optical genome mapping (OGM). The series consisted of 7 cases (M:F=1.3:1, 1-17 years, median 12). On MRI, the tumors were supratentorial in close relation to the lateral ventricles (intraventricular or iuxtaventricular), preferentially located in the occipital lobe. Two major histologic groups were identified: one (4 cases) with an overall glial appearance, indicated as "neuroepithelial" (NET) by analogy with the corresponding methylation

These authors are co-last authors: Viola Alesi and Rita Alaggio.

* Corresponding authors.
E-mail addresses: sabrina2.rossi@opbg.net (S. Rossi), evelina.miele@opbg.net (E. Miele).

https://doi.org/10.1016/j.modpat.2023.100387

EWSR1::PATZ1
gliosarcoma
MN1::PATZ1
optical genome mapping
pediatric brain tumors
ventricles

class (MC); the other (3 cases) with a predominant spindle cell sarcoma morphology, indicated as "sarcomatous" (SM). A single distinct methylation cluster encompassing both groups was identified by multidimensional scaling analysis. Despite the epigenetic homogeneity, unsupervised clustering analysis of gene expression profiles revealed 2 distinct transcriptional subgroups correlating with the histologic phenotypes. Interestingly, genes implicated in epithelial–mesenchymal transition and extracellular matrix composition were enriched in the subgroup associated to the SM phenotype. The combined use of CMA and OGM enabled the identification of chromosome 22 chromothripsis in all cases suitable for the analyses, explaining the physical association of *PATZ1* to *EWSR1* or *MN1*. Six patients are currently disease-free (median follow-up 30 months, range 12-92). One patient of the SM group developed spinal metastases at 26 months from diagnosis and is currently receiving multimodal therapy (42 months). Our data suggest that PATZ1-CNS tumors are defined by chromosome 22 chromothripsis as causative of *PATZ1* fusion, show peculiar MRI features (eg, relation to lateral ventricles, supratentorial frequently posterior site), and, although epigenetically homogenous, encompass 2 distinct histologic and transcriptional subgroups.

Introduction

In recent years, large molecular studies have led to accurate classification of undifferentiated/poorly differentiated round cell tumors in the CNS.[1] One important result was the identification of primitive neuroepithelial CNS tumors that share a common genetic background with soft tissue (ST) sarcomas.[2] Well-known examples are neoplasms carrying *BCOR*-internal tandem duplication (ITD) or *CIC* fusion.[1] In this scenario, the rearrangement of *PATZ1*, a transcriptional regulator with repressing functions known to drive a type of ST round cell sarcoma with *EWSR1*-non-ETS fusions according to 2020 WHO Classification of bone and soft tissue tumors,[3] has been more recently identified in the CNS. PATZ1-rearranged ST sarcomas (PATZ1-ST sarcomas) typically affect the trunk of young adults, and are histologically characterized by the presence of thick fibrocollagenous bands, prominent hyalinized vessels, and a polyphenotypic profile with the expression of neuroectodermal, muscular, and epithelial markers.[4-11] Differently from PATZ1-ST sarcomas, *PATZ1*-rearranged CNS tumors (PATZ1-CNS tumors) have not been included in the 2021 WHO Classification of CNS tumors,[12] due to their marked heterogeneity of histopathologic appearances and grade, as documented by the broad spectrum of diagnoses initially assigned to these cases encompassing glioneuronal tumors, astroblastomas, ependymomas, glioblastomas, pleomorphic xanthoastrocytomas, and gliosarcomas.[7,13-23] To date, information on their clinical and radiologic features and biological behavior is limited. The aim of the study was to gain accurate data on their clinicopathologic correlations and contribute to the understanding of their pathobiology. To this end, we thoroughly characterized a series of 7 pediatric CNS tumors carrying a *PATZ1* fusion and correlated the findings with their clinical, radiologic, and pathological features.

Materials and Methods

Study Series

Cases were selected based on the identification of *PATZ1* fusion either with *EWSR1* or *MN1*. Patients #1-3 and #5 underwent surgery at Bambino Gesù Children's Hospital between 2017 and 2022. Cases #4 and #6-7 were consult cases. Case #1 has been published in the form of case report[18]; case #3 has been previously included in a large series.[22] The study was approved by the institutional ethics committee. Informed consent was obtained from the patients or patients' parents in all cases.

Immunohistochemistry

Immunohistochemistry was carried out on formalin-fixed paraffin-embedded (FFPE) sections using an automated immunostainer (Dako Omnis). Primary antibodies directed against the following antigens were applied: ATRX (clone AX1, 1/100, high pH, Dianova), BRAF V600E (clone VE1, 1/50, high pH, Spring Bioscience Corp.), GFAP (polyclonal, prediluted, high pH, DAKO), H3.3K27M (polyclonal, 1/1500, high pH, Millipore), H3.3K27me3 (clone C36B11, 1/200, low pH, Cell Signaling Technology), IDH1R132H (clone DIA H09, 1/50, high pH, Dianova), Ki67 (clone MIB-1, prediluted, low pH, Dako), L1CAM (clone UJ127.11, 1/100, high pH, Sigma–Aldrich), OLIG2 (1/20, high pH, quartett), p53 (clone DO-7, prediluted, high pH, Dako), NK-κB p65 (clone D14E12,1/800, high pH, Cell Signaling Technology), Synaptophysin (clone DAK-SYNAP, prediluted, high pH, Dako), desmin (D33, 1:50, high pH, Dako), myogenin (F5D, prediluted, high pH, Dako), S100 (polyclonal, prediluted, high pH, Dako), CK CAM5.2 (CAM5.2, prediluted, low pH, BioSB,), Vimentin (V9, prediluted, high pH, Dako), SMA (1A4, high pH, prediluted, Dako), CD34 (QBend 10, prediluted, high pH, Dako) EMA (E29, prediluted, high pH, Dako), and EZHIP/CXorf67 (polyclonal, 1:250, low pH, Sigma).

RNA Sequencing

RNA was extracted from FFPE tumor tissue using Maxwell CSC FFPE RNA Extraction Kit (Promega) for the automatic extraction. RNA concentration was quantified using Qubit RNA High Sensitivity Assay kit on the Qubit fluorometer (Thermo Fisher Scientific). Three hundred nanograms of total RNA were used for NGS library preparation with SureSelect XT HS2 kit (Agilent Technologies) following the manufacturer's instructions. Raw reads were preprocessed using Fastp to remove low-quality reads and any adapters and then were aligned to the reference human genome (UCSC-Build38) using STAR (2.5.3a) algorithm.[24] The resulting alignment files were then used to identify any candidate fusion transcripts by Arriba and FusionCather pipelines.[25,26] Furthermore, case #3 was also analyzed by NGS custom Panel Archer FusionPlex (ArcherDX), according to the manufacturer's instructions, and NGS data were analyzed using Archer Data Analysis Software v6.2.3.

Expressed variants referred to as pathogenic or likely pathogenic were analyzed. Opossum was used to prepare alignments for variant calling; "SoftClipsExist True" and 'MapCutoff'=40.6 were set to reduce SNP artifacts.[27] Then variant calling was carried out using Platypus with the following settings: filterDuplicates 0 −minMapQual 0 −minFlank 0 −maxReadLength 500 −minGoodQualBases 10 −minBaseQual 20.[28]

For gene expression analysis, 5 cases of ST undifferentiated sarcomas (Ewing sarcomas carrying *EWSR1::FLI1* fusion, sarcomas carrying *BCOR::CCNB3* fusion) and 5 cases of CNS fusion-driven tumors (supratentorial ependymoma *ZFTA* fusion-positive and neuroepithelial tumors *PLAGL1*) were included as ST and CNS tumors reference categories, respectively. Notably, no cases of PATZ1-ST sarcoma were included among the ST reference cases, due to their extreme rarity in the pediatric population.

Gene counts were obtained with Cufflinks (v2.2.1), and differentially expressed genes (DEG) were identified by DEseq2 (version 3.3). Counts were centered (by subtracting their means) and normalized (dividing the values for their relative standard deviations) for both samples and genes to minimize artificially extreme values. Unsupervised analysis, which generated the heatmap, was performed using a k-mean algorithm taking in input the 1500 most variable genes across samples. Gene Set Enrichment Analysis was run on DESEQ2 normalized counts by using default parameters. Pathway and functional enrichment analyses were conducted by mean of GAGE analysis,[29] and results were annotated exploiting information from Gene ontology (GO), KEGG, and Molecular Signatures Database (MsigDB). GO, including biological process (BP), cellular component, and molecular function (MF), KEGG, Panther, and Reactome pathway enrichment analyses were carried out by WebGestalt website (http://www.webgestalt.org) for the upregulated and downregulated DEGs. Significant results were filtered by setting as cutoff a 2log2 fold change and adjusted FDR < 0.05.

Genome-Wide DNA Methylation Analyses

DNA methylation analysis was performed in all 7 cases. Genomic DNA was extracted from FFPE tissue areas with tumor cellularity greater than 70% with MagPurix FFPE DNA Extraction Kit (Zinexts, Life Science Corporation) for automatic extraction of nucleic acids.

DNA methylation profiling was performed as previously reported[30,31] according to the manufacturer's instructions of the Infinium Methylation EPIC (850k) BeadChip kit (Illumina) on the Illumina iScan Platform (Illumina).[32] Standard quality controls indicated good tumor purity, DNA quality, and bisulfite conversion. The generated raw methylation intensity data files (IDATs) were uploaded to version 12.5 of the DKFZ/Heidelberg CNS tumor methylation Classifier (https://www.molecularneuropathology.org). This platform allowed to assign a subgroup score to each tumor in the recognized MCs and to determine the presence of CNVs on the basis of methylation signal.[33] Multidimensional scaling (MDS) plot was obtained using function plotMDS of package limma[34] to calculate the Euclidean distance between samples based on the signal of all probes. In addition to the 7 cases of the series, a spinal metastasis of patient #5, a tumor residue resected through a second surgery in case #1, and a previously published CNS tumor with *EWSR1::PATZ1* fusion[17] were included in the MDS analysis. Reference groups encompassed tumor subtypes of both ST (19 cases of Ewing sarcomas and 42 cases of sarcomas with *BCOR* alterations) and CNS (11 cases of supratentorial ependymomas *ZFTA* fusion-positive, 8 cases of astroblastoma *MN1*-altered, and 7 cases of CNS tumors *BCOR*-ITD).

SNP/CGH-Array Analyses

DNA was extracted according to MagPurix FFPE DNA Extraction Kit (Zinexts, Life Science Corporation) for automatic extraction of genomic DNA. Chromosome Microarray Analysis (CMA) was performed using the Infinium CytoSNP-850K BeadChip (SNP-array, Illumina) or the Agilent 4×180K oligo-array platform (CGH-array, Agilent), according to the manufacturer's instructions. Array scanning data were generated on the Illumina iScan system or on the Agilent SureScan DX Microarray Scanner, and the results were analyzed by Bluefuse Multi 4.4 software.

Optical Genome Mapping

OGM was performed in cases #1 and #2 with available frozen tissue. Ultra-high molecular weight DNA was extracted according to the manufacturer's instructions (https://bionanogenomics.com), enzymatically labeled by the DLE-1 Enzyme, loaded on Saphyr chip, and scanned on the Saphyr instrument (Bionano Genomics). Saphyr chips were run to reach a yield of 1500 Gbp corresponding to >300× effective coverage. The Rare Variant assembly and Variant Annotation Pipeline were executed on Bionano Solve software V3.6, using Human Genome Reference Consortium GRCh38. Reporting and direct visualization of structural variants was done on Bionano Access V1.6.

Results

Clinical and Radiological Characteristics

Our series consisted of 7 PATZ1-CNS tumors. Patients were 4 boys and 3 girls, encompassing 2 infants and 5 adolescents (median age 12 years, range 17 months-17 years). As for the clinical onset, all patients had signs and symptoms of intracranial hypertension. A history of fatigue and discomfort was reported in 4 cases; hemibody tingling and neck stiffness were also each reported in 1 case. The length of symptoms varied from 2 weeks to 6 months (median 9 weeks). All patients underwent gross total resection (GTR) of the tumor, followed by adjuvant chemotherapy (HGG protocol) in the 2 infantile cases (#1-2) or by adjuvant chemotherapy and radiotherapy in 4 cases (#3, #5-7). Patient #4 did not receive any adjuvant treatment, due to the absence of overt tumor anaplasia. Six patients are currently disease-free with a median follow-up time from diagnosis of 30 months (range 12-92 months). Patient #5 developed spinal metastases at 26 months from diagnosis and underwent a spinal decompression surgery with resection of one of the metastases; she is currently receiving chemotherapy and radiotherapy (42 months).

On MRI, the lesions were large (3, 5-10 cm, median 7). All cases showed an enhancing solid component and a cystic component, which was prominent in 3 cases (#2, #3, and #5). The lesions were hyperintense on T2/FLAIR-weighted images, although the hyperintensity was only focal and mild in case #7. The majority of tumors were located in the posterior portion of the brain and involved the occipital lobe. In all cases but one, the lesions were in close proximity to the lateral ventricles (iuxtaventricular in 4 cases and intraventricular in 2), with the occipital horn being most frequently involved (#2, #3, and #6). Significant perilesional

edema was present only in case #6. Calcifications were thought to be present in 4 cases. Case #1 was also characterized by intra- and peritumoral ectatic vessels and a linear leptomeningeal enhancement involving the brain stem, the cranial nerves, and focally the spinal cord, consistent with leptomeningeal dissemination.[18] MRI features are summarized in Table 1 and illustrated in Figure 1.

Identification of Gene Fusions

RNA sequencing analysis identified *PATZ1* fusion transcript in 6 cases. In the remaining case (#3), where RNA sequencing analysis failed, a *MN1::PATZ1* in frame fusion was detected by a targeted RNA panel. The discrepancy in results between techniques may be partly explained by the low RNA quality likely linked to the age of the FFPE tissue blocks (~6 years) and the superior ability of the NGS panel to sequence the region of interest at high depth (500-1000× or higher). *PATZ1* was rearranged with *MN1* in 3 cases (#2-4) and *EWSR1* in 4 (#1, #5-7). *PATZ1* breakpoints were located within exon 1 in all cases. In line with published data, all the fusion transcripts maintained *PATZ1* exon 2-5 encoding the zinc finger domain, whereas the gene portion encoding the putative transcriptional repressor domain at the N-terminus was lacking. *MN1* breakpoints were located within intron 1, exon 1, and exon 2 (one case each). *EWSR1* breakpoints involved exon 8 in 2 cases, intron 8 and exon 6 in one case each. In case #5 a novel in frame fusion of unknown function, ie, *TAF4* (ex9)*::EYA2* (ex2), was additionally identified. See Table 2 and Supplementary Figure S1.

A few expressed variants were detected, in line with previous literature.[22] A single or a few nonrecurrent pathogenic/likely pathogenic variants were identified in 5 of 7 cases. No mutations in genes such as *IDH1/2*, *H3F3A*, *BRAF*, *CDKN2A/B*, or *TP53* were detected. See Table 2 and Supplementary Table S1.

Pathological Features

We were able to identify 2 histologic groups of tumors, which based on their predominant features are indicated from here on as "neuroepithelial" (NET group) and "sarcomatous" (SM group).

The NET group consisted of 4 cases (#1-4) with an overall glial appearance (Fig. 2 A-D). The tumors were mainly composed by oligodendroglial-like cells with round nuclei and sometimes clear cytoplasm. In one case (case #4) there were also cells showing pleomorphic nuclei and abundant cytoplasm (Fig. 2D). A striking feature in all cases was the presence of a rich capillary network with variably hyalinized walls (Fig. 2A-C). Although the tumors lacked mitotic activity in most of the areas, hypercellular foci (5%-15% of the tumor volume) with marked nuclear atypia, brisk mitoses, and pseudo-palisading or extensive necrosis were seen in 3 cases (#1-#3, Fig. 2E). These features accounted for the original diagnosis of high-grade glioma in 2 cases (cases #1-2) and anaplastic glioneural tumor in 1 (case #3). Differently, in case #4, mitotic index was homogenously low (<1 mitosis/mm^2) and overt anaplasia was absent. Microvascular proliferation was a focal feature in all cases. Rare cysts and isolated microcalcifications were also seen in 2 and 3 cases, respectively. The interface between the tumor and the adjacent cerebral parenchyma, assessable in 3 cases, was relatively sharp. All cases were diffusely positive for vimentin. Focal/patchy GFAP, OLIG2, and synaptophysin (dot-like pattern) were observed also in all cases (Fig. 2 F, G); S100 was diffuse in 2 cases and focal in the other 2; SOX10 was

Table 1
Clinical and radiological characteristics of the series

Case #	Sex	Age	Site	Maximum dimension (cm)	Relationship with lateral ventricles	T2/FLAIR hyperintensity	Enhancing components	Marked perilesional edema	Cystic component	Calcifications	Treatment	FU (m)
1	M	17 mo	Right temporo-parieto-occipital	10	Intravetricular (temporo-occipital horn)	Yes	Yes	No	Yes	Yes	GTR+CT	NED (32)
2	F	20 mo	Right parieto-occipital	8	Iuxtaventricular (occipital horn)	Yes	Yes	No	Yes (prominent)	No	GTR+CT	NED (18)
3	M	17 y	Left parieto-occipital	7	Iuxtaventricular (occipital horn)	Yes	Yes	No	Yes (prominent)	Yes	GTR+RT+CT	NED (64)
4	M	17 y	Frontal	3,5	Intravetricular (frontal horn)	Yes	Yes	No	Yes	Yes	GTR	NED (12)
5	F	12 y	Left parietal	8	Iuxtaventricular (temporal horn)	Yes	Yes	No	Yes (prominent)	No	GTR+RT+CT[a]	AWD (42)
6	F	12 y	Right parietotemporal	6	Iuxtavetricular (temporal and occipital horn)	Yes	Yes	Yes	Yes	Yes	GTR+ PT+CT	NED (29)
7	M	15 y	Left frontal	6	No	Yes (mild/focal)	Yes	No	Yes (microcysts)	No	GTR+RT+CT	NED (92)

AWD, alive with disease; CT, chemotherapy; GTR, gross total resection; NED, no evidence of disease; PT, proton therapy; RT, radiotherapy.
[a] Case #5 developed spinal metastases at 26 mo from diagnosis, underwent a spinal decompression surgery with resection of one of the metastases and has been receiving CT and RT.

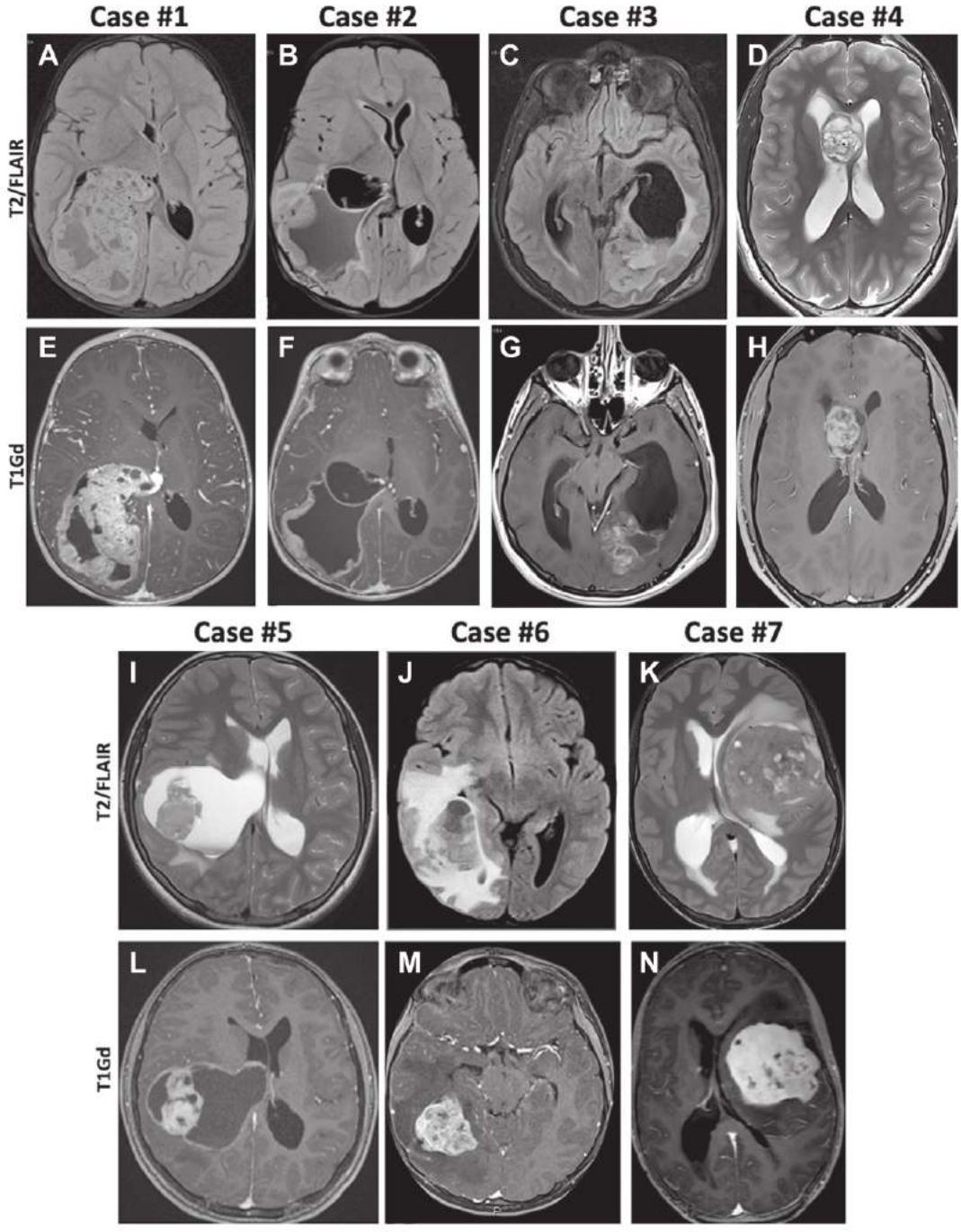

Figure 1.
MRI features: axial T2-FLAIR-weighted (A-D, I-K) and Gd T1-weighted images (E-H, L-N). The lesions were hyperintense on T2/FLAIR-weighted images and showed an enhancing solid component and a variably prominent cystic component. In cases #1-6, the tumors were in close relation with the lateral ventricles. In cases #1-3 and #5-6, the lesions were located in the posterior portion of the brain, whereas case #4 was located within the frontal horn.

present in isolated cells in 2 cases and was focal in 2; focal CD34 (Fig. 2H) and dot-like EMA expression was observed in 3 and 2 cases, respectively. Notably, 2 cases also expressed focal desmin, which was associated with myogenin and MYOD1 expression in one of them (Fig. 2I). Focal/mosaic loss of H3K27me3 expression was seen in all cases. CKCAM5.2, L1CAM, p65, H3K27M, EZHIP, IDH1-mutant, and BRAF-mutant were negative in all cases; ATRX was retained and p53 expression was observed in rare neoplastic nuclei.

The SM group (cases #5-7) shared the presence of a predominant sarcomatous spindle cell component mostly organized in long fascicles (Fig. 2J-L). Two cases (#5 and #6) showed hypercellularity, nuclear hyperchromasia, and high mitotic index throughout, consistent with a high-grade morphology (Fig. 2J, K). In case #7 hypercellular areas were intermixed with collagenized areas, and mitotic index was low throughout, consistent with a low-grade morphology (Fig. 2L). Cases #5 and #6 also featured a minor/focal overtly malignant glial component, accounting for the

Table 2
Pathological and molecular characteristics of the *PATZ1*-rearranged tumors series

Case #	Pathology group	Presence of high-grade features	PATZ1 fusion[a] (breakpoints)	Expressed variants (P/LP)	Methylation profile (v12.5)	CNV profile inferred from methylation analysis	SNP/CGH-array	Optical genome mapping
1	NET	Y (foc.)	*EWSR1* exon6-*PATZ1* exon1 (chr22:29282559-chr22:31345601)	*ERBB4*: c.1177C>T (p. R393W) LP, VAF:58%	PATZ1 fusion NET (0.99)	Segmental gains and losses at 22q	Gains and losses (chromothripsis) at 22q	Gains and losses associated with intrachromosome structural rearrangements (chromothripsis) at 22q; Segmental loss 1p36.33p12; segmental gain 1q12q44
2	NET	Y(foc.)	*MN1* intron1-*PATZ1* exon1 (chr22:27770501-chr22:31344605)	*CHD4*: c.222+1G>C LP, VAF:30%; *MTOR*: c.4107+2T>A LP, VAF: 40%; *TGFBR2*: c.458del (p. K153Sfs*35) P, VAF: 18%	PATZ1 fusion NET (0.99)	Segmental losses at 20p, 22q	Complex karyotype: multiple aneuploidies (gain of chr 7, 8, 13, 17, 21; loss of chr 4, 6, 9, 10, 14, 16, X); segmental loss 20p13p12.1 and 22q11.23q13.33	Complex karyotype: multiple aneuploidies (gain of chr 7, 8, 13, 17, 21; loss of chr 4, 6, 9, 10, 14, 16, X). Gains and losses associated with intra- and interchromosome structural rearrangements (chromothripsis) at 20p and 22q
3	NET	Y (foc.)	*MN1* exon1-*PATZ1* exon1 (chr22:28192751-chr22:31740579)	*BRCA2*: c.7390C>T (p. Q2464*) P, VAF:50%; *RB1*: c.2107-1G>A LP, VAF:33%	PATZ1 fusion NET (0.99)	Loss of 1p; gain of 1q	NA	NA
4	NET	N	*MN1* exon2-*PATZ1* exon1 (chr22:27750994-chr22:31344733)	None	PATZ1 fusion NET (0.99)	Loss of 6, 19, 22q; segmental loss at 18q	Multiple aneuploidies (gain of chr 13; loss of chr 6, 19, Y); segmental loss 18q21.2q23; chromothripsis involving chr 22	NA
5[a]	SM	Y	*EWSR1* exon8-*PATZ1* exon1 (chr22:29288786-chr22:31344697)	None	No match[b]	Segmental losses at 1p, 1q, 4, 9q,11p, 13q, 19, 20, 21q, 22; segmental gain at 1q	Monosomy of chr 4; segmental loss 1p36.33p21.3, 1q42.3q44, 11p15.5p15.4, 21q22.2q22.3; segmental gain 1q21.2q42.13; Chromothripsis involving chr 9, 13, 19, 20, 22	NA
6	SM	Y	*EWSR1* intron8-*PATZ1* exon1 (chr22:29290966-chr22:31344664)	*MSH2*: c.2091T>A (p. C697*) LP, VAF:5%	PATZ1 fusion NET (0.99)	Segmental losses at 18q, 22q; gain of chr 1q, 5, 8	Trisomy of chr 5 and 8; segmental gain 1q12q44; chromothripsis involving 18q and 22q	NA
7	SM	N	*EWSR1* exon8-*PATZ1* exon1 (chr22:29288786-chr22:31344559)	*RAD51D*: c.83-2A>G LP, VAF: 40%; *SPOP*: c.412C>T (p. R138C) P/LP, VAF:38%	No match[b]	Gain of 1q, losses at chr 22	Segmental gain 1q12q44; chromothripsis involving chr 22	NA

NA, not assessed; NET, neuroepithelial tumor; SM, sarcomatous; SR, structural rearrangements.
[a] Molecular analyses were performed on both the primary tumor and the spinal metastasis for this case (#5).
[b] Both case #5 and #7 received a score of 0.4 for the MC supratentorial ependymoma *ZFTA*-fusion positive.

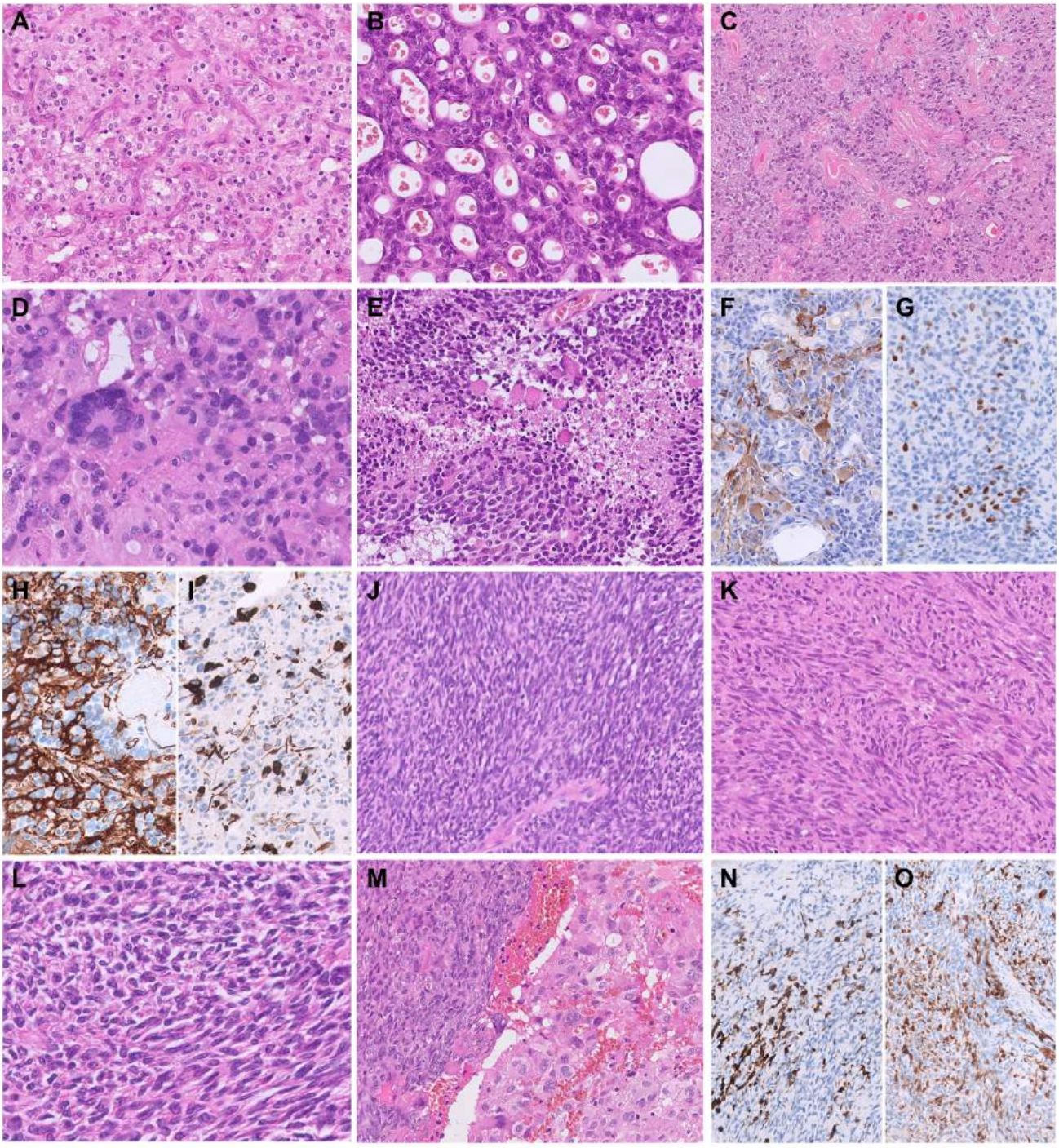

Figure 2.
Pathological features. (A-I) CNS-PATZ1 tumors, NET-group. (A-C) The lesions consisted of cells with round nuclei and sometimes clear cytoplasm and were characterized by a rich network of variably hyalinized capillaries (A: case #1; B: case #2; C: case #3). (D) In case #4, there were cells with pleomorphic nuclei. (E) Hypercellular foci with marked nuclear atypia, brisk mitoses, and pseudo-palisading necrosis were present in 3 cases. (F, G) Focal/patchy expression of GFAP (F) and OLIG2 (G) was seen in all cases. (H) Focal extravascular CD34 expression was observed in 3 cases. (I) Sparse desmin-positive cells were present in 2 cases. (J-O) CNS-PATZ1 tumors, SM-group. (J-K) High-grade sarcomatous spindle cell component of cases #5 (J) and #6 (K). (L) Low-grade sarcomatous spindle cell morphology of case #7. (M) A minor overtly malignant glial component (right) was associated with the predominant sarcomatous component (left) in cases #5-6. (N) Focal desmin expression was observed in all cases. (O) One case expressed S100.

original diagnosis of gliosarcoma (Fig. 2M). A rich hyalinized vascular network was focally present in 1 case (case #5). Microvascular proliferation was seen in 1 case (case #5). The sarcomatous component expressed diffuse vimentin and focal desmin in all 3 cases (Fig. 2N), focal GFAP in 2 cases and focal SMA, S100 (Fig. 2O), and CD34 in 1 case each; isolated cells positive for OLIG2 and synaptophysin (dot-like) were seen in 1 case each. Similarly to the NET group, H3K27me3 expression was focally lost in all cases. All the remaining stains turned out negative. See Supplementary Table S1.

CNVs and Structural Variants Detection

CNV profile was assessed by CMA (6/7), OGM (2/7), and DNA methylation analysis (7/7). CMA was informative in 6 cases and failed in 1, due to the low DNA quality (case #3). CMA demonstrated chromothripsis of chromosome 22 in 5 cases (Fig. 3A). Notably, the only case with no evidence of chromosome 22 chromothripsis (case #2) showed large deletions at 22q and 20p (Fig. 3B). Two cases, both belonging to the SM group, also showed chromothripsis of additional chromosomes, namely, chromosome 18 in case #6 and chromosomes 9, 13, 19, and 20 in case #5. Segmental chromosomal abnormalities were overall observed in 5 cases, gain at 1q being the most frequent (3 cases). Aneuploidies were present in 4 cases, with loss of chromosome 4 and gain of chromosome 13 recurring in 2 cases each. OGM could be performed in cases #1 and #2 with available frozen tissue (Fig. 3C, D). In the former, chromosome 22 were markedly altered: besides multiple gains and losses fulfilling the CNV criteria of chromothripsis, it showed 18 structural rearrangements causing physical association of *PATZ1* to *EWSR1*. 1q gain and 1p loss, which were not identified by SNP/CGH-array, were also detected (Fig. 3C). Case #2 showed a catastrophic event consistent with chromosome 22 chromothripsis (Fig. 3D), ie, a high number of intra- and interchromosomal structural rearrangements affecting chromosome 22q (26 breakpoints) and 20p (8 breakpoints), leading to physical association of *PATZ1* to *MN1*.

For case #3, the CNV profile was only inferred by DNA methylation analysis, enabling the identification of a segmental loss involving 1p and a segmental gain involving 1q. Notably, case #3 was the only case in which chromosome 22 chromothripsis could not be demonstrated. Whether this finding was related to the low quality of the starting material and/or the lower sensitivity of DNA methylation analysis in detecting CNVs compared with CMA, cannot be determined.

Combining CMA, OGM, and DNA methylation analysis, we were able to detect gain at 1q (5/7 cases) and chromosome 22 chromothripsis (6/7 cases) as recurrent segmental chromosomal abnormalities. See Table 2 and Supplementary Table S1.

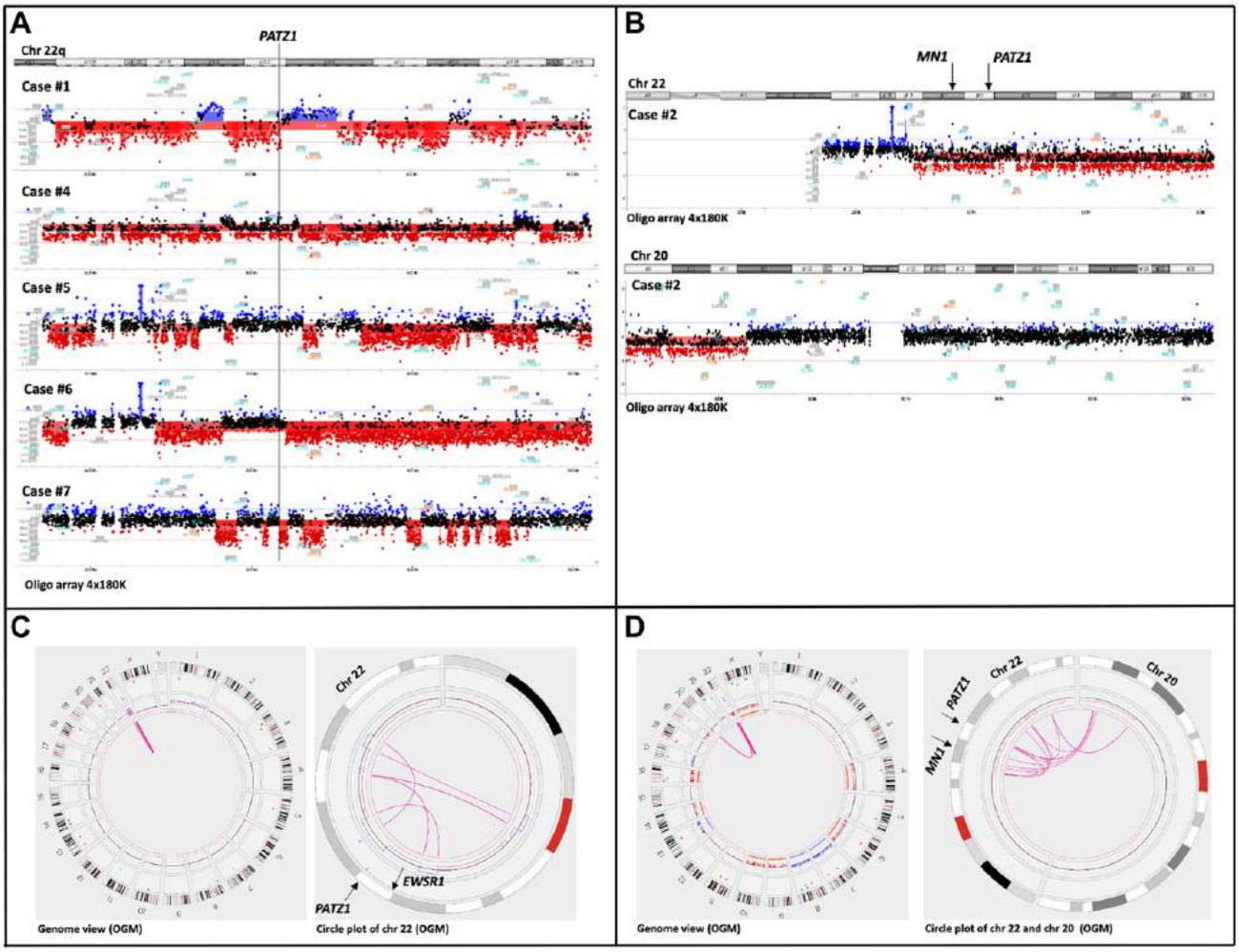

Figure 3.
Chromosome microarray analysis (CMA) and optical genome mapping (OGM). (A-B) CMA unveiled chromothripsis of chromosome 22 in 5 of 6 suitable cases (A). In the remaining case (case #2), CMA showed a segmental loss at 20p and at 22q (B). (C) In case #1, OGM revealed multiple gains and losses as well as multiple structural rearrangements within chromosome 22, a segmental loss at 1p and a segmental gain at 1q (left panel). Circle plot of chromosome 22 showing deletions, duplications, and structural intrachromosomal rearrangements accounting for 10 of the 18 breakpoints detected (right panel). (D) In case #2, OGM showed a complex karyotype with multiple aneuploidies (gain of chr 7, 8, 13, 17, 21; loss of chr 4, 6, 9, 10, 14, 16, X) and a high number of structural rearrangements affecting chromosome 22q and 20p (left panel). Circle plot of chromosomes 22 and 20 showing deletions and intra- and interchromosomal structural rearrangements associated with 26 breakpoints on chromosome 22 and 8 breakpoints on chromosome 20 (right panel). For OGM plots, red boxes, blue boxes, and purple lines indicate deletions, duplications, and structural rearrangements, respectively.

DNA Methylation Analysis

According to methylation profiling (DKFZ/Heidelberg CNS tumor methylation Classifier v12.5), all cases belonging to the NET group and 1 case of the SM group classified as "Neuroepithelial tumor with *PATZ1* fusion (novel)" with a high score (0.99) (Table 2). The remaining 2 tumors of the latter group did not match with this methylation class (MC) and both scored poorly for the MC supratentorial ependymoma ZFTA fusion-positive (score 0.4). However, by multidimensional scaling analysis, all PATZ1-CNS tumor cases clustered together in agreement with that reported by Alhalabi et al.[22] They were separated from both CNS reference categories and ST reference categories (Fig. 4A).

Gene Expression Analysis

We then investigated the transcriptomic profile of PATZ1-CNS tumors by performing a differential gene expression analysis. Unsupervised clustering analysis identified 2 major PATZ1-CNS tumor clusters: (1) a first subgroup which was proximal to the CNS reference categories and consisted of 3 NET phenotype cases (PATZ1sub_1); (2) a second subgroup close to the ST reference categories and including the SM phenotype cases and 1 NET phenotype case (PATZ1sub_2) (Fig. 4B). Notably, the latter, despite lacking histologic features of spindle cell sarcoma, expressed desmin, myogenin, and MYOD1. No clear clustering was seen either by patients' age or by fusion partner gene (Fig. 4B). The comparison of the transcriptomic profiles of PATZ1sub_1 and PATZ1sub_2 showed 1442 DEG, including 89 noncoding genes (eg, miRNA, snoRNA, and lncRNA), with striking differences in functional gene groups and pathways. Genes related to gliogenesis (eg, *adhesion G protein-coupled receptor G1*, *chondroitin sulfate proteoglycan 4*, *GFAP*, and *PAX6*) and microtubule formation (eg, genes encoding cilia and flagella-associated proteins, dynein axonemal heavy chains, and dynein regulatory complex subunits) were enriched in PATZ1sub_1 (Fig. 4C), whereas genes relevant to development, epithelial and mesenchymal differentiation (eg, *Fraser extracellular matrix complex subunit 1*, *FRAS1-related extracellular matrix protein 2*, *frizzled class receptor 2*, and *glypican 3*), and extracellular matrix components (eg, *COL26A1*, *COL27A1*, *microfibril-associated protein 4*, *fibronectin leucine rich transmembrane protein 1*, and *MMP2*) were enriched in the PATZ1sub_2 (Fig. 4D). Accordingly, pathways involved in morphogenesis, such as the WNT and the Hippo pathway, and genes implicated in epithelial–mesenchymal transition, such as *TWIST2*, *SNAI2*, and matrix metalloproteinases were specifically activated in PATZ1sub_2. We then sought to understand whether there were significant gene expression differences between each PATZ1-CNS subgroup and the closest reference group. No relevant pathways emerged from the contrast between PATZ1sub_1 and the CNS reference categories. However, besides processes related to synapsis and, to a lesser extent, gliogenesis, pathways linked to negative regulation of development were enriched in PATZ1sub_2 when compared with the ST reference categories, likely indicating a poorly committed/primitive nature of the former group. Differentially expressed genes are listed in Supplementary Table S2. Results of GO, KEGG, Panther, and Reactome analyses are summarized in Supplementary Table S3.

Discussion

Except for few cases published in the form of case reports or included in heterogenous case series,[7,13-21,23] most current knowledge on PATZ1-CNS tumors derives from a single large-scale published study.[22] In that paper, the authors identified a novel methylation cluster of 60 cases, and detected *PATZ1* fusion, with *EWSR1* or *MN1*, in the subset of them analyzed by RNA sequencing (27 cases), inferring that *PATZ1* fusion was the hallmark of the tumor cluster. They also observed chromosome 22 chromothripsis in 42% of the cases speculating on its possible role in driving the fusion formation. However, the assessment of the clinicopathologic characteristics, eg, radiologic or immunophenotypical features, was hindered by the limited access to MRI images and/or FFPE material.[22] In this study, we characterized a pediatric series of 7 cases, including 2 infants and 5 adolescents, with a rearrangement of *PATZ1* gene documented by NGS.

The lesions were all hemispheric in line with the knowledge that, although rare cerebellar and spinal examples occur,[13,15,22] the vast majority of primary PATZ1-CNS tumors are supratentorial.[13,17,22,23] Except for 1 case, they showed a close spatial relationship with the ventricles (6/7 cases). Only 4/49 cases have been indicated as iuxta-/intraventricular in the previous large published series.[22] However, this peculiar anatomical location has been observed by Siegfried et al[13] in both PATZ1-CNS cases they have described.[13] We also found a tendency for these tumors to arise in the posterior portion of the brain (5 of 7 cases), with the occipital horn being most frequently affected (3 of 7 cases).

An additional finding of our study was the identification of 2 major histologic patterns, one showing an overall glial appearance and indicated as "neuroepithelial" (NET) by analogy with the corresponding MC, and the other featuring a predominant spindle cell sarcoma morphology and indicated as "sarcomatous" (SM). To some extent, this parallels what is emerging about *ZFTA* fusion-driven CNS tumors: *ZFTA* fusion, initially described in supratentorial ependymomas, has been more recently acknowledged to drive CNS tumors with different histologies, including sarcomas, currently lacking a proper nosologic WHO definition.[35-37]

Recurrent features of the NET group were the presence of extensive low-proliferative monotonous oligo-like areas and a rich network of variably hyalinized capillaries, similar to what was previously emphasized in the 2 cases described by Sieghfried et al.[13] These characteristics are far from being specific and are encountered in other well-established entities (eg, *ZFTA* fusion-positive ependymomas)[38] and in emerging molecular subgroups of glial/glioneural tumors (eg, diffuse gliomas with *FGFR3::TACC3* fusion, anaplastic glioneuronal tumors with ATRX alteration and kinase fusion).[39,40] Furthermore, as the majority of the NET-group tumors (3/4 cases) stained for CD34 in line with previous gene expression data,[22] other CD34-positive CNS tumors, eg, polymorphous low-grade neuroepithelial tumors of the young (PLNTY), may enter in the differential diagnosis. It is of note that, different from what is seen in most glial/glioneural tumors, the expression of OLIG2 in PATZ1-CNS tumors was only focal, suggesting that a diffuse OLIG2 expression argues against this possibility. Notably, the peculiar and previously unreported immunophenotypic constellation of sparse desmin-positive cells (2/4 cases) combined with CD34 positivity (3/4 cases) and limited OLIG2 expression in the context of a pediatric iuxta-/intraventricular oligo-like tumor with a rich capillary network should prompt

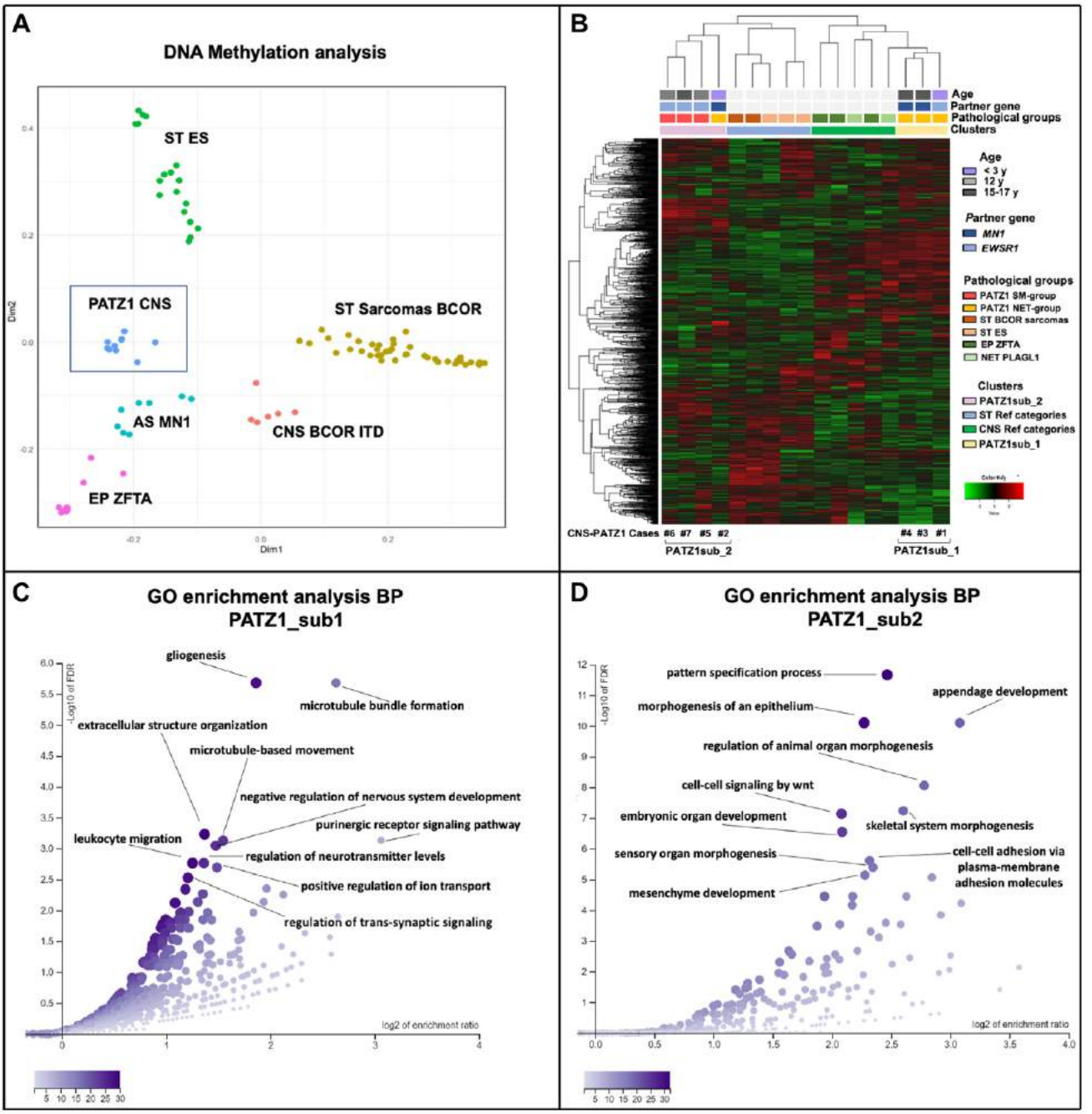

Figure 4.

DNA methylation and gene expression analyses. (A) DNA methylation analysis. Multidimensional scaling (MDS) plot showing that PATZ1-CNS tumors cluster separately from CNS and ST reference groups. CNS categories encompassed 11 cases of supratentorial ependymomas ZFTA fusion-positive (EP ZFTA), 8 cases of astroblastoma MN1-altered (AS MN1), and 7 cases of CNS tumors BCOR-internal tandem duplication (CNS BCOR-ITD). ST categories encompassed 19 cases of Ewing sarcomas (ST ES) and 42 cases of sarcomas with BCOR alterations (ST sarcomas BCOR). (B-D) Gene expression analysis. (B) Unsupervised hierarchical transcriptome clustering analysis. The heatmap portrays the expression pattern of the top 1600 genes with the highest variance (each row representing relative expression levels for a single gene, each column showing expression levels for a single sample). A close-up of the branches reveals 2 PATZ1-CNS tumor separate subgroups: (i) PATZ1_sub1 (right) consisted of 3 cases belonging to the NET-group, (ii) PATZ1_sub2 (left) included the 3 cases belonging to the SM-group and one case of the NET-group. CNS reference categories encompassed 3 cases of supratentorial ependymoma ZFTA fusion-positive (EP ZFTA) and 2 cases of neuroepithelial tumors PLAGL1 (NET PLAGL1). ST reference categories included 3 cases of *EWSR1::FLI1* rearranged Ewing sarcomas (ST ES) and 2 cases of *BCOR::CCNB3* rearranged sarcomas (ST BCOR sarcomas). (C-D) Gene ontology (GO) BP noRedundant enrichment analysis of the differentially expressed genes emerging in the contrast between PATZ1_sub2 vs PATZ1_sub1 (cutoff ≥2 log2 fold change; adjusted FDR < 0.05). BP, biological process.

molecular analysis for *PATZ1* fusions (Table 3). Remarkably, no embryonal features were seen, supporting the notion that in practical terms these tumors may be considered part of the glial group of CNS tumors rather than the embryonal.

The SM group was characterized by the presence of extensive areas of spindle cell fascicles within a collagenous stroma, sometimes associated to a minor overtly malignant glial component. Either a mesenchymal or a biphasic pattern has been previously

Table 3
Clinicopathologic elements hinting at PATZ1-CNS tumors

- Age: from infancy to adolescence
- Site: intraventricular and iuxtaventricular
- Morphology/immunophenotype/DNA methylation class (v12.5)
  - "Neuroepithelial"
    - glial features with oligo-like cellularity, rich network of variably hyalinized capillaries, low-grade features ± variably extensive high-grade foci
    - co-expression of focal GFAP, focal OLIG2 and focal synaptophysin ± expression of focal CD34, focal dot-like EMA, sparse desmin-positive cells, sparse MyoD1/myogenin-positive cells; focal/mosaic H3K27me3 loss
    - "Neuroepithelial tumor with PATZ1 fusion" (novel)
  - "Sarcomatous"
    - fibrosarcoma-like features either low-grade or high-grade ± minor overtly malignant glial component
    - expression of focal desmin ± focal SMA, focal S100, focal CD34; focal/mosaic H3K27me3 loss
    - either "No match" or "Neuroepithelial tumor with PATZ1 fusion" (novel)
- CNV: Chromosome 22 chromothripsis ± 1q gain, 1p loss
- Differential diagnoses
  - "Neuroepithelial"
    - Supratentorial ependymoma ZFTA fusion-positive, PLNTY, neurocytoma, low-grade gliomas, high-grade gliomas, glioneural tumors
  - "Sarcomatous"
    - Primary CNS sarcomas (eg, intracranial sarcomas DICER1 mutant, kinase fusion-positive spindle cell neoplasms), gliosarcomas

CNS, central nervous system; PLNTY, polymorphous low-grade neuroepithelial tumors of the young.

reported in a subset of PATZ1-CNS tumors (5/18 cases).[22] Although adult gliosarcomas are currently regarded as variants of glioblastoma IDH-wildtype,[41] pediatric gliosarcomas remain elusive. Ours and previous data indicate that at least a subset of pediatric CNS sarcomas and gliosarcomas are *PATZ1* fusion driven.[22] The differential diagnosis includes other primary CNS sarcomas featuring a fibrosarcoma-like pattern, such as intracranial sarcomas *DICER1* mutant or the emerging kinase fusion-positive spindle cell neoplasms[42-46] (Table 3). Notably, DNA methylation analysis may not always be helpful in this differential diagnostic context, as only 1 of 3 PATZ1-CNS tumors belonging to the SM group was recognized by the Classifier v12.5, and the diagnosis of such cases ultimately relies on *PATZ1* fusion identification. The extreme rarity of PATZ1-ST sarcomas in the pediatric population prevented us from directly comparing our series with the ST counterpart. However, differently from our SM group, PATZ1-ST sarcomas do not typically show a fibrosarcoma-like pattern.[7,10,11] The myriad of hyalinized branching capillaries that they usually exhibit and their monotonous cellularity with roundish nuclei are instead somewhat reminiscent of the NET phenotype of PATZ1-CNS tumors.[7,10,11]

In line with the pathological findings, we identified 2 transcriptional subgroups, namely, PATZ1sub_1 and PATZ1sub_2, roughly corresponding to the NET and SM phenotype, respectively. Not surprisingly, pathways enriched in the former subgroup were implicated in gliogenesis, followed by microtubule formation known to be relevant to axon guidance.[47] More intriguingly, genes and pathways enriched in the latter subgroup were involved in morphogenesis and epithelial–mesenchymal transition (eg, *TWIST2*, *SNAI2*, WNT pathway, and Hippo pathway)[48] as well as in extracellular matrix composition (eg, different types of collagen and matrix metalloproteinases). The expression of proteins related to epithelial–mesenchymal transition and matrix metalloproteinases has been previously shown in the majority of adult gliosarcomas by immunohistochemistry.[49] Importantly, matrix metalloproteinases may be potential therapeutic targets as demonstrated in a recent intracranial gliosarcoma model.[50]

Our histologic and transcriptional data defining 2 main PATZ1-CNS tumor subgroups may seem in contradiction with the epigenetic homogeneity of the series, as demonstrated by the identification of a single methylation cluster by t-SNE analysis in agreement with previous literature.[22] Notably, the DEG emerging from the contrast between the 2 transcriptional subgroups included 89 noncoding genes (eg, regulatory RNAs), suggesting that the separation of PATZ1-CNS tumors in 2 subsets may depend on the impairment of post-transcriptional regulation mechanisms directly interacting with mRNA.

The small size of the study precluded any consideration on the prognostic impact of the 2 phenotypes. However, intriguingly, the only patient (#5) of our series who developed a metastatic disease after 2 years from diagnosis belonged to the SM group. The lesion showed a biphasic high-grade morphology (ie, gliosarcoma), did not classify at DNA methylation analysis and demonstrated a complex karyotype with the highest number of segmental chromosomal alterations and chromosomes affected by chromothripsis (ie, chr. 9, 13, 19, 20) beside chromosome 22, likely linked to tumor progression (Table 2). Moreover, a novel *TAF4::EYA2* intrachromosomal fusion was detected in this case, likely resulting from chromothripsis of chromosome 20. Although *TAF4* and *EYA2* have been implicated in neurodevelopment[51] and gliomagenesis,[52,53] respectively, whether the novel *TAF4::EYA2* fusion may contribute to tumorigenesis remains an open question, which requires further functional studies.

Chromothripsis of chromosome 22 has been hypothesized to be the causative event of *PATZ1* fusion either with *EWSR1* or *MN1*, which all map on this chromosome.[22] However, thus far, based on CNV data inferred from DNA methylation analysis, chromosome 22 chromothripsis has been estimated to occur in approximately 42% of PATZ1-CNS tumors.[22] Remarkably, the combined implementation of CMA and OGM enabled the identification of chromosome 22 chromothripsis in 6 of 7 cases. Notably, the case that did not carry chromosome 22 chromothripsis was the one in which the CNV profile was only inferred by the DNA methylation platform, generally considered less sensitive than CMA in detecting CNV. Current chromothripsis criteria take into consideration unbalanced copy number changes, as chromothripsis is defined by the presence of >10 CNV affecting a limited number of chromosomes.[54] Notably, in case #2 chromosome 22q showed a large deletion and did not fulfill the CNV-based chromothripsis criteria. However, OGM documented a high number of intra- and interchromosomal structural rearrangements, providing evidence of a genomic catastrophic event involving chromosome 22 even in this case. Chromothripsis is generally regarded as an early event linked to tumor initiation through amplification of oncogenes, deletion of oncosuppressor genes, or generation of gene fusions.[55] Although in specific molecular tumor subgroups chromothripsis is associated with a poor prognosis (eg, SHH medulloblastomas in the context of Li-Fraumeni syndrome), it is found also in low-grade glioneural tumors with favorable outcome.[56]

Although a small study, our data indicate that PATZ1-CNS tumors are defined by the presence of chromosome 22 chromothripsis as causative of *PATZ1* rearrangement, show peculiar MRI features and, although epigenetically homogenous, encompass 2 distinct phenotypical and transcriptional subgroups, one showing an overall glial appearance and the other presenting a predominant sarcomatous component (Table 3). Whether these phenotypes may have a different influence on patient outcomes and whether they may represent separate entities remains to be elucidated.

Acknowledgments

The authors thank Mr. Gabriele Bacile for iconography preparation and Claudia Nardini for technical support.

Author Contributions

S.R., R.A., V.A., and E.M. were involved in the study conception. S.R., S.A., M.P.G., P.P.L., S.B., C.T, V.A., S.G., F.D., E.M., S.P., I.G., G.S.C., E.P., G.D., A.M., A.C., E.V., S.D., E.S., G.C., L.M., F.T., F.M, M.Z., E.G., R.L., A.C., and D.Q. contributed to acquisition of data. S.R., S.B., C.T., E.M., V.A., S.G., G.S.C., C.G., and V.C. performed analysis and interpretation of data. S.R., S.B., V.A., and E.M. were involved in the drafting of manuscript. C.G., A.M., E.M., V.A., M.G., R.A., V.C., A.N., and A.O.M. made critical revision. All authors approved the final version of the manuscript to be published.

Data Availability

NGS data, methylation profiling, chromosomal microarray analysis, and OGM data are available on request from the authors.

Funding

Ministry of Health, funds 2020 to A.O.M. (202105_INNOV_Onet).

Declaration of Competing Interest

The authors declare no conflicts of interest.

Ethics Approval and Consent to Participate

This study was approved by the ethics committee. Written consent to the publication of the case details was given by patients or patients' parents.

Supplementary Material

The online version contains supplementary material available at https://doi.org/10.1016/j.modpat.2023.100387.

References

1. Sturm D, Orr BA, Toprak UH, et al. New brain tumor entities emerge from molecular classification of CNS-PNETs. *Cell*. 2016;164:1060–1072. https://doi.org/10.1016/j.cell.2016.01.015
2. Pizzimenti C, Gianno F, Gessi M. Expanding the spectrum of "mesenchymal" tumors of the central nervous system. *Pathologica*. 2022;114:455–464. https://doi.org/10.32074/1591-951X-826
3. Bridge JA, ed. Round cell sarcoma with EWSR1on-TS fusions. In: *WHO Classification of Tumours Editorial Board. Soft Tissue and Bone Tumours*. WHO classification of tumours series, 5th ed. Vol. 3. Lyon (France): International Agency for Research on Cancer; 2020:326–329. https://publications.iarc.fr/588
4. Mastrangelo T, Modena P, Tornielli S, et al. A novel zinc finger gene is fused to EWS in small round cell tumor. *Oncogene*. 2000;19:3799–3804. https://doi.org/10.1038/sj.onc.1203762
5. Watson S, Perrin V, Guillemot D, et al. Transcriptomic definition of molecular subgroups of small round cell sarcomas. *J Pathol*. 2018;245:29–40. https://doi.org/10.1002/path.5053
6. Chougule A, Taylor MS, Nardi V, et al. Spindle and round cell sarcoma with *EWSR1-PATZ1* gene fusion: a sarcoma with polyphenotypic differentiation. *Am J Surg Pathol*. 2019;43:220–228. https://doi.org/10.1097/PAS.0000000000001183
7. Bridge JA, Sumegi J, Druta M, et al. Clinical, pathological, and genomic features of EWSR1-PATZ1 fusion sarcoma. *Mod Pathol*. 2019;32:1593–1604. https://doi.org/10.1038/s41379-019-0301-1
8. Park KW, Cai Y, Benjamin T, Qorbani A, George J. Round cell sarcoma with *EWSR1-PATZ1* gene fusion in the neck: case report and review of the literature. *Laryngoscope*. 2020;130:E833–E836. https://doi.org/10.1002/lary.28554
9. Tsuda Y, Zhang L, Meyers P, Tap WD, Healey JH, Antonescu CR. The clinical heterogeneity of round cell sarcomas with EWSR1/FUS gene fusions: impact of gene fusion type on clinical features and outcome. *Genes Chromosomes Cancer*. 2020;59:525–534. https://doi.org/10.1002/gcc.22857
10. Michal M, Rubin BP, Agaimy A, et al. EWSR1-PATZ1-rearranged sarcoma: a report of nine cases of spindle and round cell neoplasms with predilection for thoracoabdominal soft tissues and frequent expression of neural and skeletal muscle markers. *Mod Pathol*. 2021;34:770–785. https://doi.org/10.1038/s41379-020-00684-8
11. Folpe AL. 'I Can't Keep Up!': an update on advances in soft tissue pathology occurring after the publication of the 2020 World Health Organization classification of soft tissue and bone tumours. *Histopathology*. 2022;80:54–75. https://doi.org/10.1111/his.14460
12. Louis DN, ed. Introduction to CNS tumours In: *WHO Classification of Tumours Editorial Board. Central Nervous System Tumours*. WHO classification of tumours series, 5th ed. Vol 6. Lyon (France): International Agency for Research on Cancer International Agency for Research on Cancer; 2021:8–14. https://publications.iarc.fr/601
13. Siegfried A, Rousseau A, Maurage CA, et al. *EWSR1-PATZ1* gene fusion may define a new glioneuronal tumor entity. *Brain Pathol*. 2019;29:53–62. https://doi.org/10.1111/bpa.12619
14. Johnson A, Severson E, Gay L, et al. Comprehensive genomic profiling of 282 pediatric low- and high-grade gliomas reveals genomic drivers, tumor mutational burden, and hypermutation signatures. *Oncologist*. 2017;22:1478–1490. https://doi.org/10.1634/theoncologist.2017-0242
15. Pei J, Zhao X, Patchefsky AS, et al. Clinical application of RNA sequencing in sarcoma diagnosis: an institutional experience. *Medicine*. 2019;98:e16031. https://doi.org/10.1097/MD.0000000000016031
16. Qaddoumi I, Orisme W, Wen J, et al. Genetic alterations in uncommon low-grade neuroepithelial tumors: BRAF, FGFR1, and MYB mutations occur at high frequency and align with morphology. *Acta Neuropathol*. 2016;131:833–845. https://doi.org/10.1007/s00401-016-1539-z
17. Lopez-Nunez O, Cafferata B, Santi M, et al. The spectrum of rare central nervous system (CNS) tumors with EWSR1-non-ETS fusions: experience from three pediatric institutions with review of the literature. *Brain Pathol*. 2021;31:70–83. https://doi.org/10.1111/bpa.12900
18. Rossi S, Barresi S, Giovannoni I, et al. Expanding the spectrum of EWSR1-PATZ1 rearranged CNS tumors: an infantile case with leptomeningeal dissemination. *Brain Pathol*. 2021;31:e12934. https://doi.org/10.1111/bpa.12934
19. Stichel D, Schrimpf D, Casalini B, et al. Routine RNA sequencing of formalin-fixed paraffin-embedded specimens in neuropathology diagnostics identifies diagnostically and therapeutically relevant gene fusions. *Acta Neuropathol*. 2019;138:827–835. https://doi.org/10.1007/s00401-019-02039-3
20. Burel-Vandenbos F, Pierron G, Thomas C, Reynaud S, Gregoire V, Duhil de Benaze G. A polyphenotypic malignant paediatric brain tumour presenting a MN1-PATZ1 fusion, no epigenetic similarities with CNS high-grade neuroepithelial tumour with MN1 Alteration (CNS HGNET-MN1) and related to PATZ1-fused sarcomas. *Neuropathol Appl Neurobiol*. 2020;46:506–509. https://doi.org/10.1111/nan.12626
21. Chadda KR, Holland K, Scoffings D, et al. Genomics England Research Consortium. A rare case of paediatric astroblastoma with concomitant MN1-GTSE1 and EWSR1-PATZ1 gene fusions altering management. *Neuropathol Appl Neurobiol*. 2021;47:882–888. https://doi.org/10.1111/nan.12701
22. Alhalabi KT, Stichel D, Sievers P, et al. PATZ1 fusions define a novel molecularly distinct neuroepithelial tumor entity with a broad histological spectrum. *Acta Neuropathol*. 2021;142:841–857. https://doi.org/10.1007/s00401-021-02354-8
23. Tauziède-Espariat A, Chotard G, le Loarer F, et al. A novel LARGE1-AFF2 fusion expanding the molecular alterations associated with the methylation class of neuroepithelial tumors with PATZ1 fusions. *Acta Neuropathol Commun*. 2022;10:15. https://doi.org/10.1186/s40478-022-01317-8
24. Chen S, Zhou Y, Chen Y, Gu J. fastp: an ultra-fast all-in-one FASTQ preprocessor. *Bioinformatics*. 2018;34:i884–i890. https://doi.org/10.1093/bioinformatics/bty560
25. Uhrig S, Ellermann J, Walther T, et al. Accurate and efficient detection of gene fusions from RNA sequencing data. *Genome Res*. 2021;31:448–460. https://doi.org/10.1101/gr.257246.119

26. Nicorici D, Satalan M, Edgren H, et al. FusionCatcher - a tool for finding somatic fusion genes in paired-end RNA-sequencing data. Preprint. Posted online November 19, 2014. biorxiv011650v1. https://doi.org/10.1101/011650
27. Oikkonen L, Lise S. Making the most of RNA-seq: pre-processing sequencing data with Opossum for reliable SNP variant detection. *Wellcome Open Res*. 2017;2:6. https://doi.org/10.12688/wellcomeopenres.10501.2
28. Rimmer A, Phan H, Mathieson I, et al. Integrating mapping-, assembly- and haplotype-based approaches for calling variants in clinical sequencing applications. *Nat Genet*. 2014;46:912–918. https://doi.org/10.1038/ng.3036
29. Luo W, Friedman MS, Shedden K, Hankenson KD, Woolf PJ. GAGE: generally applicable gene set enrichment for pathway analysis. *BMC Bioinformatics*. 2009;10:161. https://doi.org/10.1186/1471-2105-10-161
30. Miele E, De Vito R, Ciolfi A, et al. DNA Methylation profiling for diagnosing undifferentiated sarcoma with capicua transcriptional receptor (CIC) alterations. *Int J Mol Sci*. 2020;21:1818. https://doi.org/10.3390/ijms21051818
31. Salgado CM, Alaggio R, Ciolfi A, et al. Pediatric BCOR-altered tumors from soft tissue/kidney display specific DNA methylation profiles. *Mod Pathol*. 2023;36:100039. https://doi.org/10.1016/j.modpat.2022.100039
32. Lopez-Nunez O, Alaggio R, John I, et al. Melanotic neuroectodermal tumor of infancy (MNTI) and pineal anlage tumor (PAT) harbor A medulloblastoma signature by DNA methylation profiling. *Cancers)*. 2021;13:706. https://doi.org/10.3390/cancers13040706
33. Capper D, Jones DTW, Sill M, et al. DNA methylation-based classification of central nervous system tumours. *Nature*. 2018;555:469–474. https://doi.org/10.1038/nature26000
34. Ritchie ME, Phipson B, Wu D, et al. limma Powers differential expression analyses for RNA-sequencing and microarray studies. *Nucleic Acids Res*. 2015;43:e47. https://doi.org/10.1093/nar/gkv007
35. Zheng T, Ghasemi DR, Okonechnikov K, et al. Cross-species genomics reveals oncogenic dependencies in ZFTA/C11orf95 fusion-positive supratentorial ependymomas. *Cancer Discov*. 2021;11:2230–2247. https://doi.org/10.1158/2159-8290.CD-20-0963
36. Tauziède-Espariat A, Siegfried A, Nicaise Y, et al. Supratentorial non-RELA, ZFTA-fused ependymomas: a comprehensive phenotype genotype correlation highlighting the number of zinc fingers in ZFTA-NCOA1/2 fusions. *Acta Neuropathol Commun*. 2021;9:135. https://doi.org/10.1186/s40478-021-01238-y
37. Kresbach C, Neyazi S, Schüller U. Updates in the classification of ependymal neoplasms: The 2021 WHO Classification and beyond. *Brain Pathol*. 2022;32:e13068. https://doi.org/10.1111/bpa.13068
38. Figarella-Branger D, Lechapt-Zalcman E, Tabouret E, et al. Supratentorial clear cell ependymomas with branching capillaries demonstrate characteristic clinicopathological features and pathological activation of nuclear factor-κB signaling. *Neuro Oncol*. 2016;18:919–927. https://doi.org/10.1093/neuonc/now025
39. Métais A, Tauziède-Espariat A, Garcia J, et al, Biopathology RENOCLIP-LOC network. Clinico-pathological and epigenetic heterogeneity of diffuse gliomas with FGFR3::TACC3 fusion. *Acta Neuropathol Commun*. 2023;11:14. https://doi.org/10.1186/s40478-023-01506-z
40. Bogumil H, Sill M, Schrimpf D, et al. Glioneuronal tumor with ATRX alteration, kinase fusion and anaplastic features (GTAKA): a molecularly distinct brain tumor type with recurrent NTRK gene fusions. *Acta Neuropathol*. 2023;145:667–680. https://doi.org/10.1007/s00401-023-02558-0
41. Brat DJ, von Deimling A, eds. Glioblastoma, IDH-ildtype. In: *WHO Classification of Tumours Editorial Board. Central Nervous System Tumours*. WHO classification of tumours series, 5th ed. Vol. 6. Lyon (France): International Agency for Research on Cancer; 2021:39–68. https://publications.iarc.fr/601
42. Koelsche C, Mynarek M, Schrimpf D, et al. Primary intracranial spindle cell sarcoma with rhabdomyosarcoma-like features share a highly distinct methylation profile and DICER1 mutations. *Acta Neuropathol*. 2018;136:327–337. https://doi.org/10.1007/s00401-018-1871-6
43. Lee JC, Villanueva-Meyer JE, Ferris SP, et al. Primary intracranial sarcomas with DICER1 mutation often contain prominent eosinophilic cytoplasmic globules and can occur in the setting of neurofibromatosis type 1. *Acta Neuropathol*. 2019;137:521–525. https://doi.org/10.1007/s00401-019-01960-x
44. Kamihara J, Paulson V, Breen MA, et al. DICER1-associated central nervous system sarcoma in children: comprehensive clinicopathologic and genetic analysis of a newly described rare tumor. *Mod Pathol*. 2020;33:1910–1921. https://doi.org/10.1038/s41379-020-0516-1
45. Tauziède-Espariat A, Duchesne M, Baud J, et al. NTRK-rearranged spindle cell neoplasms are ubiquitous tumours of myofibroblastic lineage with a distinct methylation class. *Histopathology*. 2023;82:596–607. https://doi.org/10.1111/his.14842
46. Tauziède-Espariat A, Hasty L, Métais A, Varlet P. Mesenchymal non-meningothelial tumors of the central nervous system: a literature review and diagnostic update of novelties and emerging entities. *Acta Neuropathol Commun*. 2023;11:22. https://doi.org/10.1186/s40478-023-01522-z
47. Lasser M, Tiber J, Lowery LA. The role of the microtubule cytoskeleton in neurodevelopmental disorders. *Front Cell Neurosci*. 2018;12:165. https://doi.org/10.3389/fncel.2018.00165
48. Ismagulov G, Hamidi S, Sheng G. Epithelial-mesenchymal transition drives three-dimensional morphogenesis in mammalian early development. *Front Cell Dev Biol*. 2021;9:639244. https://doi.org/10.3389/fcell.2021.639244
49. Nagaishi M, Paulus W, Brokinkel B, et al. Transcriptional factors for epithelial-mesenchymal transition are associated with mesenchymal differentiation in gliosarcoma. *Brain Pathol*. 2012;22:670–676. https://doi.org/10.1111/j.1750-3639.2012.00571.x
50. Pinheiro L, Perdomo-Pantoja A, Casaos J, et al. Captopril inhibits matrix metalloproteinase-2 and extends survival as a temozolomide adjuvant in an intracranial gliosarcoma model. *Clin Neurol Neurosurg*. 2021;207, 106771. https://doi.org/10.1016/j.clineuro.2021.106771
51. Janssen BDE, van den Boogaard MH, Lichtenbelt K, et al. De novo putative loss-of-function variants in TAF4 are associated with a neuro-developmental disorder. *Hum Mutat*. 2022;43:1844–1851. https://doi.org/10.1002/humu.24444
52. Zhang G, Dong Z, Gimple RC, et al. Targeting EYA2 tyrosine phosphatase activity in glioblastoma stem cells induces mitotic catastrophe. *J Exp Med*. 2021;218:e20202669. https://doi.org/10.1084/jem.20202669
53. Wen Z, Liang C, Pan Q, Wang Y. Eya2 overexpression promotes the invasion of human astrocytoma through the regulation of ERK/MMP9 signaling. *Int J Mol Med*. 2017;40:1315–1322. https://doi.org/10.3892/ijmm.2017.3132
54. Korbel JO, Campbell PJ. Criteria for inference of chromothripsis in cancer genomes. *Cell*. 2013;152:1226–1236. https://doi.org/10.1016/j.cell.2013.02.023
55. Voronina N, Wong JKL, Hübschmann D, et al. The landscape of chromothripsis across adult cancer types. *Nat Commun*. 2020;11:2320. https://doi.org/10.1038/s41467-020-16134-7
56. Prabowo S, van Thuijl HF, Scheinin I, et al. Landscape of chromosomal copy number aberrations in gangliogliomas and dysembryoplastic neuroepithelial tumours. *Neuropathol Appl Neurobiol*. 2015;41:743–755. https://doi.org/10.1111/nan.12235